Inorganic Chemistry
Article

Inorg. Chem. **2010**, *49*, 8977–8985 **8977**
DOI: 10.1021/ic101257b

Theoretical Study of Excited States of Pyrazolate- and Pyridinethiolate-Bridged Dinuclear Platinum(II) Complexes: Relationship between Geometries of Excited States and Phosphorescence Spectra

Ken Saito,[†] Yoshihide Nakao,[†] Keisuke Umakoshi,[‡] and Shigeyoshi Sakaki*[,§]

[†]*Department of Molecular Engineering, Graduate School of Engineering, Kyoto University, Nishikyo-ku, Kyoto 615-8510, Japan,* [‡]*Department of Applied Chemistry, Faculty of Engineering, Nagasaki University, Bunkyo-machi, Nagasaki 852-8251, Japan, and* [§]*Institute for Integrated Cell-Material Sciences, Kyoto University, Ushinomiya-cho,Yoshida, Sakyo-ku, Kyoto 606-8501, Japan*

Received June 24, 2010

Dinuclear platinum(II) complexes $[Pt_2(\mu\text{-pz})_2(bpym)_2]^{2+}$ (**1**; pz = pyrazolate and bpym = 2,2′-bipyrimidine) and $[Pt_2(\mu\text{-pyt})_2(ppy)_2]$ (**2**; pyt = pyridine-2-thiolate and Hppy = 2-phenylpyridine) were theoretically investigated with density functional theory (DFT) to clarify the reasons why the phosphorescence of **1** is not observed in the acetonitrile (CH_3CN) solution at room temperature (RT) but observed in the solid state at RT and why the phosphorescence of **2** is observed in both the CH_3CN solution and the solid state at RT. The S_1 and T_1 states of **1** in the CH_3CN solution are assigned as a metal−metal-to-ligand charge-transfer (MMLCT) excited state. Their geometries are C_{2v} symmetrical, in which spin−orbit interaction between the S_1 and T_1 excited states is absent because the direct product of irreducible representations of the singly occupied molecular orbitals (SOMOs) of these excited states and the orbital angular momentum (l) operator involved in the Hamiltonian for spin−orbit interaction does not belong to the a_1 representation. As a result, the $S_1 \rightarrow T_1$ intersystem crossing hardly occurs, leading to the absence of $T_1 \rightarrow S_0$ phosphorescence in the CH_3CN solution at RT. In the solid state, the geometry of the S_1 state does not reach the global minimum but stays in the C_1-symmetrical local minimum. This S_1 excited state is assigned as a mixture of the ligand-centered $\pi-\pi^*$ excited state and the metal-to-ligand charge-transfer excited state. Spin−orbit interaction between the S_1 and T_1 excited states operates to induce the $S_1 \rightarrow T_1$ intersystem crossing because the direct product of the irreducible representations of the SOMOs of these excited states and the l operator belongs to the “a” representation. As a result, $T_1 \rightarrow S_0$ phosphorescence occurs in the solid state. In **2**, the S_1 and T_1 excited states are assigned as the MMLCT excited state. Their geometries are C_2-symmetrical in both the CH_3CN solution and the solid state, in which spin−orbit interaction between the S_1 and T_1 states operates to induce the $S_1 \rightarrow T_1$ intersystem crossing because the direct product of the irreducible representations of the SOMOs and the l operator belongs to the “a” representation. Thus, $T_1 \rightarrow S_0$ phosphorescence occurs in both the CH_3CN solution and the solid state at RT, unlike **1**.

1. Introduction

Emissive transition-metal complexes have drawn a lot of interest because they are potentially useful to optical materials such as light-emitting devices, photochemical sensors, and biological labeling probes.[1−3] In particular, 5d transition-metal complexes such as iridium[2] and platinum[2a,3−8] complexes have been well-investigated because large phosphorescence spectra are often observed in these complexes.

---

*To whom correspondence should be addressed. E-mail: sakaki@moleng.kyoto-u.ac.jp.

(1) Selected reviews for emissive complexes applied to optical materials: (a) Amendola, V.; Fabbrizzi, L.; Foti, F.; Licchelli, M.; Mangano, C.; Pallavicini, P.; Poggi, A.; Sacchi, D.; Taglietti, A. *Coord. Chem. Rev.* **2006**, *250*, 273. (b) Rogers, C. W.; Wolf, M. O. *Coord. Chem. Rev.* **2002**, *233*−*234*, 341. (c) Keefe, M. H.; Benkstein, K. D.; Hupp, J. T. *Coord. Chem. Rev.* **2000**, *205*, 201.

(2) Selected reviews for emissive iridium complexes applied to optical materials: (a) Evans, R. C.; Douglas, P.; Winscom, C. J. *Coord. Chem. Rev.* **2006**, *250*, 2093. (b) Marin, V.; Holder, E.; Hoogenboom, R.; Schubert, U. S. *Chem. Soc. Rev.* **2007**, *36*, 618. (c) Lo, K. K.-W.; Hui, W.-K.; Chung, C.-K.; Tsang, K. H.-K.; Lee, T. K.-M.; Li, C.-K.; Lau, J. S.-Y.; Ng, D. C.-M. *Coord. Chem. Rev.* **2006**, *250*, 1724. (d) Lo, K. K.-W.; Hui, W.-K.; Chung, C.-K.; Tsang, K. H.-K.; Ng, D. C.-M.; Zhu, N.; Cheung, K.-K. *Coord. Chem. Rev.* **2005**, *249*, 1434.

(3) Selected reviews for emissive platinum complexes applied to optical materials: (a) Kato, M. *Bull. Chem. Soc. Jpn.* **2007**, *80*, 287. (b) Yam, V. W.-W. *Acc. Chem. Res.* **2002**, *35*, 555. (c) Hissler, M.; McGarrah, J. E.; Connick, W. B.; Geiger, D. K.; Cummings, S. D.; Eisenberg, R. *Coord. Chem. Rev.* **2000**, *208*, 115. (d) Paw, W.; Cummings, S. D.; Mansour, M. A.; Connick, W. B.; Geiger, D. K.; Eisenberg, R. *Coord. Chem. Rev.* **1998**, *171*, 125.

(4) Selected review for the fundamental study of emissive platinum complexes:Wong, K. M.-C.; Hui, C.-K.; Yu, K.-L.; Yam, V. W.-W. *Coord. Chem. Rev.* **2002**, *229*, 123.

(5) Umakoshi, K.; Kimura, K.; Kim, Y. H.; Arikawa, Y.; Ohnishi, M.; Ishizaka, S.; Kitamura, N. Private communication. Absorption and emission spectra of **1** are presented in the Supporting Information; see Figures S1 and S2.

(6) Koshiyama, T.; Omura, A.; Kato, M. *Chem. Lett.* **2004**, *33*, 1386.

(7) Ma, B.; Li, J.; Djurovich, P. I.; Yousufuddin, M.; Bau, R.; Thompson, M. E. *J. Am. Chem. Soc.* **2005**, *127*, 28.

© 2010 American Chemical Society

Published on Web 08/30/2010

Scheme 1

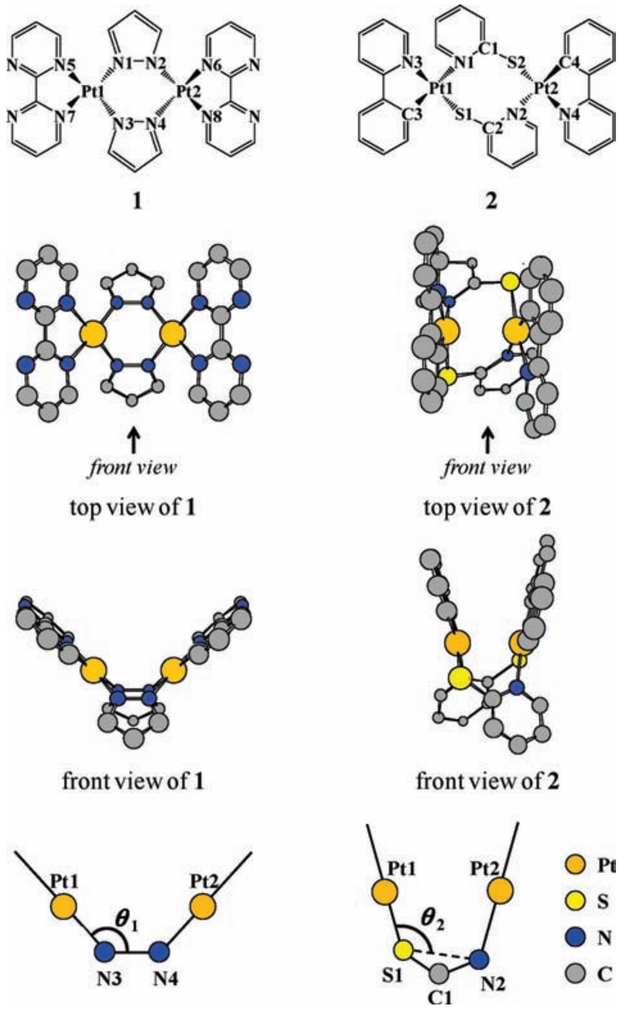

Recently, multinuclear transition-metal complexes have been investigated in many experimental works[1c,2a,3−8] because they exhibit a variety of phosphorescence spectra. For instance, the phosphorescence spectrum of pyrazolate-bridged dinuclear platinum(II) complex $[Pt_2(\mu\text{-pz})_2(bpym)_2]^{2+}$ (**1**; pz = pyrazolate and bpym = 2,2′-bipyrimidine; see Scheme 1)[5] is observed in the solid state but not in the acetonitrile (CH_3CN) solution. However, that of pyridinethiolate-bridged dinuclear platinum(II) complex $[Pt_2(\mu\text{-pyt})_2(ppy)_2]$ (**2**; pyt = pyridine-2-thiolate and Hppy = 2-phenylpyridine; Scheme 1)[6] is observed in both the solid state and the CH_3CN solution. It is of considerable interest to clarify the reasons why these moderately different bridging and chelating ligands induce the above-mentioned differences in phosphorescence behavior between **1** and **2**. The phosphorescence spectrum of **2** was experimentally discussed in terms of the geometries and electronic structures of the singlet ground state (S_0) and the lowest-energy triplet excited state (T_1).[6] However, the reasons for the above-mentioned differences between **1** and **2** have not been discussed yet. It is worth investigating theoretically the ground and excited states of **1** and **2** to understand their phosphorescence spectra and elucidate the reasons why the phosphorescence behavior is different between them.

In this study, we theoretically investigated pz- and pyt-bridged dinuclear platinum(II) complexes **1** and **2** and discussed the geometries and electronic structures of the S_0 ground state and the lowest-energy singlet and triplet excited states (S_1 and T_1, respectively). We also discussed whether or not spin−orbit interaction between the S_1 and T_1 states operates, because this spin−orbit interaction plays an important role in the $S_1 \rightarrow T_1$ intersystem crossing. Our main purposes here are (i) to present a theoretical understanding of the geometries, electronic structures, and phosphorescence spectra of **1** and **2** and (ii) to clarify the reasons why the phosphorescence spectrum of **1** is absent but that of **2** is present in the CH_3CN solution and why those of **1** and **2** are observed in the solid state.

2. Computational Details

We employed two basis set systems (basis I and II) in this study. In basis I, core electrons (up to 4f) of platinum were replaced with the relativistic effective core potentials (ECPs) proposed by Hay and Wadt[9] and its valence electrons were represented by the (541/541/111/1) basis set.[9−11] The 6-31G* basis sets[12] were used for hydrogen, carbon, nitrogen, and sulfur. In basis II, valence electrons of platinum were represented by the (5311/5311/111/1) basis set[9−11] with the same ECPs as those of basis I. The cc-pVDZ basis sets[13] were used for hydrogen, carbon, nitrogen, and sulfur.

Geometries of **1** and **2** in the S_0 ground state were optimized by density functional theory (DFT) with basis I, where the B3PW91 functional[14,15] was employed. The geometries in the S_1 and T_1 excited states were optimized with the unrestricted (U)DFT method. Because the singly occupied molecular orbital (SOMO) bearing an α-spin electron is different from that bearing a β-spin electron in the S_1 state, the spin symmetry of the evaluated wave function is broken in the UDFT calculation.[16] In this meaning, the UDFT calculation of the S_1 state is called broken-symmetry (BS)DFT. It is also called permuted orbitals (PO)DFT in several cases.[17] We ascertained that all optimized geometries exhibited no imaginary frequency. The potential energy curves (PECs) of **1** and **2** were evaluated as a function of the Pt−Pt distance in the S_0, S_1, and T_1 states, where all geometrical parameters were optimized at each Pt−Pt distance.

The energy of phosphorescence is calculated here as the energy difference between the S_0 and T_1 states at the T_1-optimized geometry. The total energies, orbital energies, and Mulliken charges were evaluated with the DFT(B3PW91)/basis II//DFT(B3PW91)/basis I method.[18] The solvent effect of the CH_3CN solution was taken into consideration by the

---

(8) Saito, K.; Nakao, Y.; Sakaki, S. *Inorg. Chem.* **2008**, *47*, 4329.

(9) Hay, P. J.; Wadt, W. R. *J. Chem. Phys.* **1985**, *82*, 299.

(10) Couty, M.; Hall, M. B. *J. Comput. Chem.* **1996**, *17*, 1359.

(11) Ehlers, A. W.; Böhme, M.; Dapprich, S.; Gobbi, A.; Höllwarth, A.; Jonas, V.; Köhler, K. F.; Stegmann, R.; Veldkamp, A.; Frenking., G. *Chem. Phys. Lett.* **1993**, *208*, 111.

(12) (a) Hehre, W. J.; Ditchfield, R.; Pople, J. A. *J. Chem. Phys.* **1972**, *56*, 2257. (b) Hariharan, P. C.; Pople, J. A. *Theor. Chim. Acta* **1973**, *28*, 213. (c) Francl, M. M.; Pietro, W. J.; Hehre, W. J.; Binkley, J. S.; Gordon, M. S.; DeFrees, D. J.; Pople, J. A. *J. Chem. Phys.* **1982**, *77*, 3654.

(13) (a) Dunning, T. H., Jr. *J. Chem. Phys.* **1989**, *90*, 1007. (b) Woon, D. E.; Dunning, T. H., Jr. *J. Chem. Phys.* **1993**, *98*, 1358.

(14) (a) Becke, A. D. *Phys. Rev. A* **1988**, *38*, 3098. (b) Becke, A. D. *J. Chem. Phys.* **1993**, *98*, 5648.

(15) Perdew, J. P.; Wang, Y. *Phys. Rev. B* **1992**, *45*, 13244.

(16) The S^2 values were evaluated to be 1.01, 1.01, and 1.02 for the S_1-optimized geometries $\mathbf{1S_{1a}}$, $\mathbf{1S_{1b}}$, and $\mathbf{2S_{1a}}$, respectively, where the *S* means the spin momentum operator. These evaluated values indicate that the spin symmetries of these evaluated S_1 wave functions are broken. On the contrary, the spin symmetry was not broken at all in the S_0 wave function and little broken in the T_1 wave function. The S^2 values were evaluated to be 0.00, 0.00, 2.01, 2.03, and 2.01 for the $\mathbf{1S_0}$, $\mathbf{2S_0}$, $\mathbf{1T_{1a}}$, $\mathbf{1T_{1b}}$, and $\mathbf{2T_{1a}}$ geometries, respectively.

(17) Gräfenstein, J.; Kraka, E.; Filatov, M.; Cremer, D. *Int. J. Mol. Sci.* **2002**, *3*, 360.

Table 1. Several Important Optimized Bond Lengths (Å), Bond Angles (deg), Dihedral Angles (deg),[a] π*(bpym), dσ*(Pt−Pt), and π(bpym) Orbital Energies (eV),[b,c] and Molecular Volumes (Å^3) of **1**

	exptl values of a similar complex[d]	**1S$_0$**	**1S$_{1a}$**	**1S$_{1b}$**	**1T$_{1a}$**	**1T$_{1b}$**
r(Pt1−Pt2)	3.376	3.451	2.791	3.441	2.777	3.480
r(Pt1−N1)	2.093	2.012	2.024	1.996	2.024	2.009
r(Pt1−N3)	2.071	2.012	2.024	2.020	2.024	2.023
r(Pt2−N2)	1.998	2.012	2.024	2.020	2.024	2.014
r(Pt2−N4)	2.019	2.012	2.024	2.011	2.024	2.009
r(Pt1−N5)	2.005	2.036	2.023	2.030	2.022	2.026
r(Pt1−N7)	2.021	2.036	2.023	1.996	2.022	1.976
r(Pt2−N6)	1.986	2.036	2.023	2.037	2.022	2.038
r(Pt2−N8)	2.005	2.036	2.023	2.027	2.022	2.034
a(N1−Pt1−N3)	86.1	85.3	85.4	85.9	85.3	86.3
a(N2−Pt2−N8)	84.8	85.3	85.4	85.1	85.3	85.1
a(N5−Pt1−N7)	81.6	80.1	80.6	80.9	80.5	81.5
a(N6−Pt2−N8)	81.4	80.1	80.6	80.1	80.5	80.1
d(Pt1−N1−N3−N4)[e]	132.6	135.1	118.9	137.2	118.7	136.9
d(Pt1−N3−N1−N2)	−132.3	−135.1	−118.9	−134.7	−118.7	−138.7
d(Pt2−N2−N4−N3)	−138.8	−135.1	−118.9	−132.6	−118.7	−135.1
d(Pt2−N4−N2−N1)	126.2	135.1	118.9	135.1	118.7	133.3
ε[π*(bpym)]		−8.46	−8.97	−8.88	−8.99	−9.00
ε[dσ*(Pt−Pt)]		−12.47	−11.73	−12.49	−11.79	−12.53
ε[π(bpym)]		−13.77	−13.94	−13.76	−13.95	−13.76
molecular volume		585	606	586	604	585

[a] Geometries were optimized with the B3PW91/basis I method in vacuo. [b] These orbitals are shown in Figure 1. [c] Orbital energies were calculated in the S$_0$ state with the B3PW91/basis II//B3PW91/basis I mehod. [d] Experimental bond lengths, bond angles, and bond dihedral angles of **3** reported by Thompson et al. (ref 7). Note that **3** is not C_{2v} but C_s symmetrical. [e] This dihedral angle corresponds to θ_1 in Scheme 1.

polarizable continuum model (PCM).[19] The united-atom topological model of the universal force-field method (UA0)[19b,20] was employed to estimate the molecular volume and construct a molecular cavity in the PCM calculation.

The DFT calculations were performed by the *Gaussian 03* (revision C.02) program package.[21] Molecular orbitals were drawn by the *MOLEKEL* (version 4.3) program.[22]

3. Results and Discussion

3.1. Equilibrium Geometries and Electronic Structures of [Pt$_2$(μ-pz)$_2$(bpym)$_2$]$^{2+}$ (1) in the S$_0$, S$_1$, and T$_1$ States. Important optimized geometrical parameters of the S$_0$ equilibrium geometry of **1** (**1S$_0$**) are shown in Table 1. This geometry is C_{2v}-symmetrical, which is clearly shown by the fact that the Pt1−N1, Pt1−N3, Pt2−N2, and Pt2−N4 bond lengths are the same (2.012 Å). The Pt1−Pt2 distance (3.451 Å) and the Pt1−N1−N3−N4 dihedral angle θ_1 (135.1°) are similar to those of [Pt$_2$(μ-pz)$_2$(dfppy)$_2$] [**3**; dfppy = 2-(2,4-difluorophenyl)pyridine] recently reported by Thompson et al.,[7] in which the Pt−Pt distance is 3.376 Å and the θ_1 dihedral angle is 132.6°; see Scheme 1 for the definition of θ_1. These results indicate that the geometry of **1** is mainly determined by the μ-pz ligand.

We optimized geometries of the S$_1$ and T$_1$ excited states against various Pt−Pt distances and found two equilibrium structures in these excited states: one bearing the short Pt−Pt distance (**1S$_{1a}$** and **1T$_{1a}$** geometries) and the other bearing the long Pt−Pt distance (**1S$_{1b}$** and **1T$_{1b}$** geometries), as shown in Table 1; see the Pt−Pt distances of **1S$_{1a}$** (2.791 Å), **1T$_{1a}$** (2.777 Å), **1S$_{1b}$** (3.441 Å), and **1T$_{1b}$** (3.480 Å). All of these optimized geometries have no imaginary frequency. Interestingly, the **1S$_{1b}$** and **1T$_{1b}$** geometries are C_1-symmetrical; see the Pt1−N1, Pt1−N3, Pt2−N2, and Pt2−N4 bond lengths of 1.996, 2.020, 2.020, and 2.011 Å, respectively, in the **1S$_{1b}$** geometry and 2.009, 2.023, 2.014, and 2.009 Å, respectively, in the **1T$_{1b}$** geometry. On the other hand, the **1S$_{1a}$** and **1T$_{1a}$** geometries are C_{2v}-symmetrical; their Pt1−N1, Pt1−N3, Pt2−N2, and Pt2−N4 bond lengths are the same (2.024 Å). The **1S$_{1a}$** geometry bearing the short Pt−Pt distance is the global minimum of the S$_1$ state. However, the **1T$_{1b}$** geometry bearing the long Pt−Pt distance is the global minimum of the T$_1$ state, although the energy difference between the global and local minima is small; they are 0.16 and 0.04 eV in the S$_1$ and T$_1$ states, respectively. Previously, similar global and local minima were found in the T$_1$ state of **3**.[8]

In the **1S$_{1a}$** and **1T$_{1a}$** geometries, the dσ*(Pt−Pt) and π*(bpym) orbitals are singly occupied, where the dσ*(Pt−Pt) orbital mainly consists of the dσ−dσ antibonding orbital between two platinum nuclei and the π*(bpym) orbital represents the π* orbital of the bpym ligand, as shown in Figure 1. In other words, one-electron excitation occurs from the dσ*(Pt−Pt) orbital to the π*(bpym) orbital in these excited states. Thus, this electronic structure is assigned as the metal−metal-to-ligand charge-transfer (MMLCT) excited state. The same assignment was experimentally and theoretically reported for the T$_1$ excited state at the T$_1$ global minimum of **3**.[7,8] Because one-electron excitation occurs from the antibonding dσ*(Pt−Pt) orbital to the π*(bpym) orbital in these excited states, the bonding interaction between two platinum nuclei becomes stronger; note that the formal Pt−Pt bond order is 0.5 in the **1S$_{1a}$** and **1T$_{1a}$** geometries but 0.0 in the **1S$_0$** geometry. As a result, the Pt1−Pt2

---

(18) Orbital energies and energies of phosphorescences are little different between basis I and II, as shown in Tables S3 and S4 in the Supporting Information. This suggests that both basis sets are reliable.

(19) (a) Mennucci, B.; Tomasi, J. *J. Chem. Phys.* **1997**, *106*, 5151. (b) Cancès, M. T.; Mennucci, B.; Tomasi, J. *J. Chem. Phys.* **1997**, *107*, 3032. (c) Cossi, M.; Barone, V.; Mennucci, B.; Tomasi, J. *Chem. Phys. Lett.* **1998**, *286*, 253. (d) Tomasi, J.; Persico, M. *Chem. Rev.* **1994**, *94*, 2027.

(20) Rappé, A. K.; Casewit, C. J.; Colwell, K. S.; Goddard, W. A., III; Skiff, W. M. *J. Am. Chem. Soc.* **1992**, *114*, 10024.

(21) Pople, J. A.; et al. *Gaussian 03*, revision C.02; Gaussian, Inc.: Wallingford, CT, 2004.

(22) (a) Flükiger, P.; Lüthi, H. P.; Portmann, S.; Weber, J. *MOLEKEL*, version 4.3; Scientific Computing: Manno, Switzerland, 2000−2002. (b) Portmann, S.; Lüthi, H. P. *Chimia* **2000**, *54*, 766.

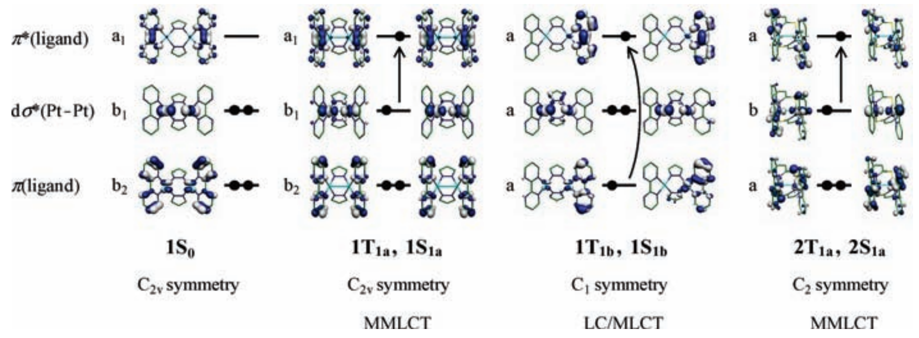

Figure 1. Several important molecular orbitals of the $\mathbf{1S_0}$, $\mathbf{1T_{1a}}$, $\mathbf{1S_{1a}}$, $\mathbf{1T_{1b}}$, $\mathbf{1S_{1b}}$, $\mathbf{2T_{1a}}$, and $\mathbf{2S_{1a}}$ geometries. Irreducible representations (a_1, b_1, b_2, a, and b) of these molecular orbitals are also represented. H atoms are omitted for brevity.

distance becomes shorter and the θ_1 dihedral angle becomes smaller in the $\mathbf{1S_{1a}}$ and $\mathbf{1T_{1a}}$ geometries than in the $\mathbf{1S_0}$ geometry, as shown in Table 1. The other geometrical parameters of the $\mathbf{1S_{1a}}$ and $\mathbf{1T_{1a}}$ geometries such as the Pt1−N1 distance, the N1−Pt1−N3 bond angle, and the bond distances in the bpym and pz moieties are not significantly different from those of the $\mathbf{1S_0}$ geometry; see Table 1 and Table S1 in the Supporting Information for these geometrical parameters.

In the $\mathbf{1S_{1b}}$ and $\mathbf{1T_{1b}}$ geometries, the π(bpym) and π*(bpym) orbitals are singly occupied, as shown in Figure 1. The π(bpym) orbital somewhat interacts with the d orbital of platinum, while the π*(bpym) orbital little interacts. Thus, the electronic structures of the $\mathbf{1S_{1b}}$ and $\mathbf{1T_{1b}}$ geometries are assigned as a mixture of the ligand-centered $\pi-\pi$* excited state and the metal-to-ligand charge transfer excited state (LC/MLCT). The same assignment was experimentally[7] and theoretically[8] reported for the local minimum geometry of the T_1 excited state of **3**. As shown in Figure 1, the dσ*(Pt−Pt) orbital is doubly occupied in the $\mathbf{1S_{1b}}$ and $\mathbf{1T_{1b}}$ geometries, unlike in the $\mathbf{1S_{1a}}$ and $\mathbf{1T_{1a}}$ geometries. As a result, the dσ−dσ bonding interaction is absent in these $\mathbf{1S_{1b}}$ and $\mathbf{1T_{1b}}$ geometries, like in the $\mathbf{1S_0}$ geometry, leading to little changes in the Pt1−Pt2 distance and the θ_1 dihedral angle when going from the $\mathbf{1S_0}$ geometry to the $\mathbf{1S_{1b}}$ and $\mathbf{1T_{1b}}$ geometries, as shown in Table 1. Also, the other geometrical parameters are little different among the $\mathbf{1S_{1b}}$, $\mathbf{1T_{1b}}$, and $\mathbf{1S_0}$ geometries; see Table 1 and Table S1 in the Supporting Information. This means that the $\mathbf{1S_{1b}}$ and $\mathbf{1T_{1b}}$ geometries resemble well the $\mathbf{1S_0}$ geometry.

The differences in the electronic structure and geometry between the MMLCT ($\mathbf{1S_{1a}}$ and $\mathbf{1T_{1a}}$) and LC/MLCT ($\mathbf{1S_{1b}}$ and $\mathbf{1T_{1b}}$) excited states are explained in terms of dependences of the π*(bpym), dσ*(Pt−Pt), and π(bpym) orbital energies on the Pt−Pt distance. The dσ*(Pt−Pt) orbital energy becomes higher as the Pt−Pt distance becomes shorter because the antibonding overlap between the two dσ(Pt) orbitals increases with a decrease in the Pt−Pt distance; see Figure 1 for the dσ*(Pt−Pt) orbital. On the other hand, the π(bpym) and π*(bpym) orbital energies little depend on the Pt−Pt distance. Actually, the dσ*(Pt−Pt) orbital exists at much higher energy in the $\mathbf{1S_{1a}}$ and $\mathbf{1T_{1a}}$ geometries than in the $\mathbf{1S_{1b}}$ and $\mathbf{1T_{1b}}$ geometries, while the π(bpym) and π*(bpym) orbital energies are little different among the $\mathbf{1S_{1a}}$, $\mathbf{1S_{1b}}$, $\mathbf{1T_{1a}}$, and $\mathbf{1T_{1b}}$ geometries; see Table 1 for the orbital energies. Thus, the energy difference between the π*(bpym) and dσ*(Pt−Pt) orbitals is much smaller in the $\mathbf{1S_{1a}}$ (2.76 eV) and $\mathbf{1T_{1a}}$ (2.80 eV) geometries than in the $\mathbf{1S_{1b}}$ (3.61 eV) and $\mathbf{1T_{1b}}$ (3.53 eV) geometries. These are the reasons why the $\mathbf{1S_{1a}}$ and $\mathbf{1T_{1a}}$ geometries bearing the short Pt−Pt distance take the MMLCT [dσ*(Pt−Pt) → π*(bpym)] excited state but the $\mathbf{1S_{1b}}$ and $\mathbf{1T_{1b}}$ geometries bearing the long Pt−Pt distance take the LC/MLCT [π(bpym) + d(Pt) → π*(bpym)] excited state.

Table 2. Several Important Optimized Bond Lengths (Å), Bond Angles (deg), Dihedral Angles (deg),[a] π*(ppy), dσ*(Pt−Pt), and π(ppy) Orbital Energies (eV),[b,c] and Molecular Volumes (Å^3) of **2**

	expt[d]	$\mathbf{2S_0}$	$\mathbf{2S_{1a}}$	$\mathbf{2T_{1a}}$
r(Pt1−Pt2)	2.849	2.944	2.680	2.675
r(Pt1−N1)	2.142	2.180	2.194	2.194
r(Pt2−N2)	2.142	2.180	2.194	2.194
r(Pt1−N3)	2.038	2.061	2.052	2.050
r(Pt2−N4)	2.036	2.061	2.052	2.050
r(Pt1−S1)	2.284	2.316	2.330	2.331
r(Pt2−S2)	2.284	2.316	2.330	2.331
r(Pt1−C3)	1.987	1.992	1.998	1.997
r(Pt2−C4)	1.983	1.992	1.998	1.997
a(N1−Pt1−S1)	90.4	88.4	88.1	88.0
a(N2−Pt2−S2)	90.3	88.4	88.1	88.0
a(N3−Pt1−C3)	81.1	80.7	81.0	81.0
a(N4−Pt2−C4)	81.3	80.7	81.0	81.0
d(Pt1−N1−S1−N2)[e]	105.4	108.3	103.8	103.7
d(Pt2−N2−S2−N1)	106.3	108.3	103.8	103.7
ε[π*(ppy)]		−1.72	−1.84	−1.84
ε[dσ*(Pt−Pt)]		−4.71	−4.37	−4.36
ε[π(ppy)]		−6.52	−6.37	−6.37
molecular volume		712	698	697

[a] Geometries were optimized with the B3PW91/basis I method in vacuo. [b] These orbitals are shown in Figure 1. [c] Orbital energies were calculated in the S_0 state with the B3PW91/basis II//B3PW91/basis I method. [d] Reference 6. [e] This dihedral angle corresponds to θ_2 in Scheme 1.

3.2. Equilibrium Geometries and Electronic Structures of [$\mathbf{Pt_2(\mu\text{-}pyt)_2(ppy)_2}$] (2) in the $\mathbf{S_0}$, $\mathbf{S_1}$, and $\mathbf{T_1}$ States. The optimized geometry ($\mathbf{2S_0}$) of **2** in the S_0 state agrees well with the experimental one,[6] as shown in Table 2, except that the Pt1−Pt2 distance (2.944 Å) is moderately longer and the Pt1−N1−S1−N2 dihedral angle θ_2 (108.3°) is moderately larger than their experimental values (2.849 Å and 105.4°); see Scheme 1 for Pt1, Pt2, N1, etc., and the definition of θ_2. It is noted that the Pt−Pt distance of **2** is much shorter than that of **1** and two Pt−ppy planes of **2** are almost parallel to each other, unlike two Pt−bpym planes of **1**; see Scheme 1. These significant differences in the geometry between $\mathbf{1S_0}$ and $\mathbf{2S_0}$ arise from the direction of the lone-pair orbitals of the pyt and pz ligands. As

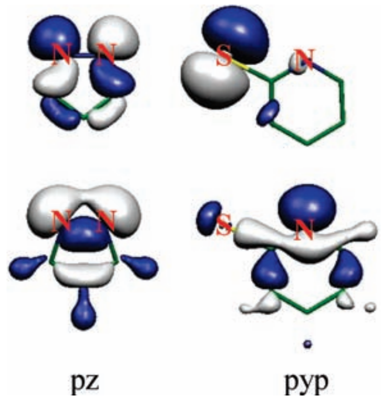

Figure 2. Lone-pair orbitals of pz and pyt. H atoms are omitted for brevity.

shown in Figure 2, two nitrogen lone-pair orbitals of pz expand toward the outside but the nitrogen and sulfur lone-pair orbitals of pyt expand in nearly parallel fashion to each other or toward rather the inside. Optimized geometrical parameters of **2** in the S_1 and T_1 global minima ($\mathbf{2S_{1a}}$ and $\mathbf{2T_{1a}}$) are also presented in Table 2. The Pt1−Pt2 distances of the $\mathbf{2S_{1a}}$ and $\mathbf{2T_{1a}}$ geometries are much shorter, and their θ_2 dihedral angles are much smaller than those of the $\mathbf{2S_0}$ geometry. These results are understood in terms of the electronic structures of the $\mathbf{2S_{1a}}$ and $\mathbf{2T_{1a}}$ geometries: SOMOs are the dσ*(Pt−Pt) and π*(ppy) orbitals in the $\mathbf{2S_{1a}}$ and $\mathbf{2T_{1a}}$ geometries, as shown in Figure 1. This means that one-electron excitation occurs from the dσ*(Pt−Pt) orbital to the π*(ppy) orbital in the $\mathbf{2S_{1a}}$ and $\mathbf{2T_{1a}}$ geometries, which leads to the presence of the Pt−Pt bonding interaction. Hence, the Pt1−Pt2 distance becomes shorter and the θ_2 dihedral angle becomes smaller in the $\mathbf{2S_{1a}}$ and $\mathbf{2T_{1a}}$ geometries than in the $\mathbf{2S_0}$ geometry. These S_1 and T_1 excited states of **2** are assigned as the MMLCT excited state.

The $\mathbf{2S_{1a}}$ and $\mathbf{2T_{1a}}$ geometries are similar to the $\mathbf{1S_{1a}}$ and $\mathbf{1T_{1a}}$ geometries, respectively, except that the $\mathbf{2S_{1a}}$ and $\mathbf{2T_{1a}}$ geometries are C_2-symmetrical, unlike the C_{2v}-symmetrical $\mathbf{1S_{1a}}$ and $\mathbf{1T_{1a}}$ geometries, as shown in Tables 1 and 2 and Figure 1. One important difference between **1** and **2** is that the local minimum geometry is absent in the S_1 and T_1 excited states of **2** but present in those of **1**, as discussed above. This is interpreted in terms of the lone-pair orbital of the bridging ligand. The sulfur and nitrogen lone-pair orbitals of pyt expand toward rather the inside (Figure 2), as discussed above, leading to the short Pt−Pt distance (2.944 Å) even in the S_0 ground state. Because the LC/MLCT excited state is possible when the Pt−Pt distance is long, the LC/MLCT excited state cannot be formed in **2**. A similar feature is observed in **3**; the T_1 local minimum of the LC/MLCT state bearing the long Pt−Pt distance cannot be formed in **3** when bulky substituents are introduced to the pz ligand, as reported previously,[7,8] because the bulky substituents decrease the Pt−Pt distance. On the basis of these results, it is concluded that the pyt ligand plays a role to decrease the Pt−Pt distance, like the pz ligand bearing a bulky substituent in **3**.

3.3. S_0, T_1, and S_1 PECs of 1 and 2.

The PECs of the S_0, S_1, and T_1 states of **1** are evaluated as a function of the Pt−Pt distance in vacuo, as shown in Figure 3a, where the geometry was optimized at each Pt−Pt distance with the B3PW91/basis I method. In the S_1 and T_1 PECs, a small but nonnegligible barrier exists around the Pt−Pt distance of 3 Å. The S_1 and T_1 states take the MMLCT excited state in the Pt−Pt distance shorter than 3 Å and the LC/MLCT excited state in the Pt−Pt distance longer than 3 Å.

The energy difference is very small (0.02 eV) between the $\mathbf{1S_{1a}}$ and $\mathbf{1T_{1a}}$ geometries but somewhat large (0.22 eV) between the $\mathbf{1S_{1b}}$ and $\mathbf{1T_{1b}}$ geometries. These results are interpreted in terms of the exchange integral, as follows: The energy difference between the S_1 and T_1 states is approximately represented by twice the exchange integral, when the molecular orbitals are not very different between these two states:[23]

$$E(\mathrm{S_1}) - E(\mathrm{T_1}) \approx 2(\mathrm{XY}|\mathrm{YX}) \tag{1}$$

where $E(\mathrm{S_1})$ and $E(\mathrm{T_1})$ are the energies of the S_1 and T_1 states, respectively, X and Y are SOMOs of the S_1 and T_1 states, and (XY|YX) is an exchange integral. In general, the exchange integral becomes large when the SOMOs (X and Y) are localized in one moiety. In the $\mathbf{1S_{1b}}$ and $\mathbf{1T_{1b}}$ geometries, the SOMOs are localized on the right-hand side of the molecule, as shown in Figure 1. In the $\mathbf{1S_{1a}}$ and $\mathbf{1T_{1a}}$ geometries, on the other hand, the SOMOs are delocalized on the whole molecule. As a result, the energy difference between the $\mathbf{1S_{1a}}$ and $\mathbf{1T_{1a}}$ geometries is smaller than that between the $\mathbf{1S_{1b}}$ and $\mathbf{1T_{1b}}$ geometries.

The S_0, T_1, and S_1 PECs of **1** were reevaluated in the CH_3CN solution by the PCM method at the B3PW91/basis I level, where the optimized geometries in vacuo were employed. Although the ^{3}MMLCT-optimized geometry ($\mathbf{1T_{1a}}$) is slightly more unstable than the ^{3}LC/MLCT-optimized geometry ($\mathbf{1T_{1b}}$) in vacuo (Figure 3a), the former is considerably more stable than the latter in the CH_3CN solution, as shown in Figure 3b. To elucidate the reason of this solvent effect, we will examine here how much polarization occurs in the MMLCT and LC/MLCT excited states. The LC/MLCT state mainly consists of localized π−π* excitation in one bpym and moderate CT excitation from the Pt−pz moiety to bpym in one pz−Pt−bpym moiety, as shown in Figure 1. On the other hand, the MMLCT state consists of CT excitation in two pz−Pt−bpym moieties. These features of the MMLCT and LC/MLCT states are consistent with the Mulliken charges of the $\mathbf{1T_{1a}}$, $\mathbf{1T_{1b}}$, and $\mathbf{1S_0}$ geometries. In the $\mathbf{1T_{1b}}$ geometry, the Pt1 atom is somewhat and the pz(N1^N2) is moderately more positively charged (+0.10 and +0.06, respectively) than those in the $\mathbf{1S_0}$ geometry, as shown in Table 3, where the pz(N1^N2) means the pz ligand including N1 and N2 atoms. Consistent with these Mulliken charges, the bpym(N6^N8) is much more negatively charged (−0.19) in the $\mathbf{1T_{1b}}$ geometry than in the $\mathbf{1S_0}$ geometry. On the other hand, the Mulliken charges of the Pt2 atom, pz(N3^N4), and bpym(N5^N7) are little different between the $\mathbf{1T_{1b}}$ and $\mathbf{1S_0}$ geometries. In the $\mathbf{1T_{1a}}$ geometry, two Pt atoms and two pz ligands are much more positively charged (+0.10 and +0.11) and two bpym

---

[23] Szabo, A.; Ostlund, N. S. *Modern Quantum Chemistry: Introduction to Advanced Electronic Structure Theory*; Dover Publications, Inc.: New York, 1996.

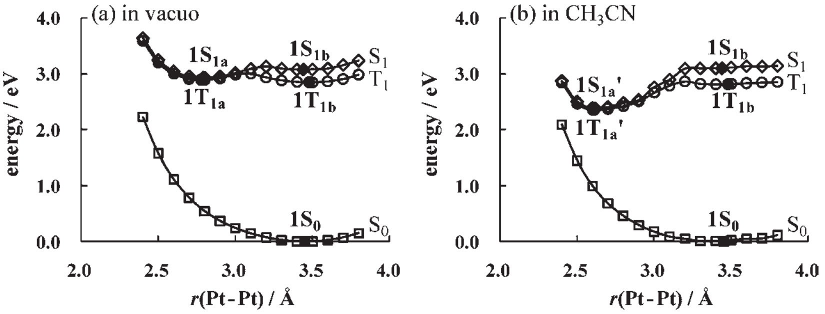

Figure 3. PECs of the S_0, T_1, and S_1 states of **1** vs the Pt−Pt distance. Geometries were optimized with the B3PW91/basis I method at each Pt−Pt distance. It is noted that the energy difference between the T_1 and S_0 curves does not correspond to the energy of phosphorescence because the T_1 curve represents the energy of the T_1-optimized geometry and the S_0 curve represents the energy of the S_0-optimized geometry. The energy of phosphorescence corresponds to the energy difference between the T_1 and S_0 states at the T_1-optimized geometry.

Table 3. Changes of the Mulliken Charges When Going from the S_0-Optimized Geometry to the S_1- or T_1-Optimized Geometries of **1** and **2**

	Pt1	Pt2	pz(N1^N2)[a]	pz(N3^N4)	bpym-(N5^N7)	bpym-(N6^N8)
			In Vacuo			
$1S_{1a}$	+0.10	+0.10	+0.11	+0.11	−0.21	−0.21
$1T_{1a}$	+0.10	+0.10	+0.11	+0.11	−0.21	−0.21
$1S_{1b}$	+0.10	+0.01	+0.07	+0.02	+0.02	−0.22
$1T_{1b}$	+0.10	+0.01	+0.06	+0.01	+0.01	−0.19
			In CH_3CN			
$1S_{1a}$	+0.16	+0.16	+0.10	+0.10	−0.26	−0.26
$1T_{1a}$	+0.16	+0.16	+0.10	+0.10	−0.26	−0.26
$1S_{1a}'$	+0.17	+0.17	+0.10	+0.10	−0.27	−0.27
$1T_{1a}'$	+0.17	+0.17	+0.10	+0.10	−0.27	−0.27
$1S_{1b}$	+0.11	+0.02	+0.12	+0.04	+0.02	−0.31
$1T_{1b}$	+0.13	+0.01	+0.10	+0.02	+0.02	−0.28

	Pt1	Pt2	thp-(N1^S2)	thp-(N2^S1)	ppy-(N3^C3)	ppy-(N4^C4)
			In Vacuo			
$2S_{1a}$	+0.05	+0.05	+0.09	+0.09	−0.14	−0.14
$2T_{1a}$	+0.04	+0.04	+0.09	+0.09	−0.13	−0.13
			In CH_3CN			
$2S_{1a}$	+0.10	+0.10	+0.10	+0.10	−0.20	−0.20
$2T_{1a}$	+0.09	+0.09	+0.10	+0.10	−0.19	−0.19

[a] pz(N1^N2) means the pz ligand including N1 and N2 atoms; see Scheme 1.

ligands are much more negatively charged (−0.21) than those in the **$1S_0$** geometry. These results indicate that CT more likely occurs in the MMLCT state than in the LC/MLCT state, leading to the formation of a more polarized electron distribution in the MMLCT excited state than in the LC/MLCT state. As a result, the MMLCT state is more stabilized by the polar CH_3CN solvent than the LC/MLCT state. This is the main reason why the **$1T_{1a}$** geometry becomes a global minimum in the CH_3CN solution. In the S_1 excited state, the ^{1}MMLCT state is also much more stabilized by the CH_3CN solution than the ^{1}LC/MLCT state, like in the T_1 states, as shown in Figure 3b.

It should be noted that the Mulliken charges change much more in the CH_3CN solution than in vacuo when going from the **$1S_0$** geometry to the **$1S_{1a}$** and **$1T_{1a}$** geometries, as shown in Table 3; for example, the Mulliken charge of Pt1 increases by +0.16 in the CH_3CN solution but by +0.10 in vacuo when going from the **$1S_0$** geometry to the **$1S_{1a}$** and **$1T_{1a}$** geometries. This means that the CH_3CN solvent accelerates CT from the Pt moiety to the π^* of bpym in the MMLCT excited state. As a result, MMLCT excitation decreases more the electron density of the dσ^*(Pt−Pt) orbital in the CH_3CN solution than in vacuo, which decreases more the Pt−Pt distances of the ^{1}MMLCT and ^{3}MMLCT excited states to 2.620 and 2.610 Å, respectively, in the CH_3CN solution than in vacuo, as shown in Figure 2b. These equilibrium geometries in the CH_3CN solution are named as **$1S_{1a}'$** and **$1T_{1a}'$** hereafter.

The S_0, T_1, and S_1 PECs of **2** are shown in Figure 4a,b. Only the global minimum exists in the S_1 and T_1 PECs of **2**, but no local minimum exists in these excited states, as mentioned above. The same names, **$2S_{1a}$** and **$2T_{1a}$**, are employed for these global minimum geometries in both vacuo and the CH_3CN solution, because these geometries in the CH_3CN solution are almost the same as those in vacuo, unlike the **$1S_{1a}$** and **$1T_{1a}$** geometries; for instance, the Pt−Pt distance is 2.680 and 2.675 Å for the **$2S_{1a}$** and **$2T_{1a}$** geometries, respectively, in both vacuo and the CH_3CN solution; see Table 2 and Figure 4.[24]

3.4. Reasons Why the Phosphorescence Spectrum of 1 Is Observed in the Solid State but Not in the CH_3CN Solution.

In **1**, $S_0 \rightarrow S_1$ photoexcitation occurs at 3.50 eV (353 nm).[5] This excitation energy is evaluated to be 3.39 eV as the energy difference between the S_0 and S_1 states at the S_0 equilibrium geometry. This $S_0 \rightarrow S_1$ photoexcitation yields the S_1 state, with the S_0 equilibrium geometry (**$1S_0$**) due to the Franck−Condon principle. It is likely that the geometry of the S_1 state changes to the C_{2v}-symmetrical global minimum **$1S_{1a}'$** geometry in CH_3CN, because the CH_3CN solution is flexible enough not to suppress the geometry change. The electronic structure of the S_1 state changes from the LC/MLCT state to the MMLCT one when going from the **$1S_0$** geometry to the **$1S_{1a}'$** one. In the **$1S_{1a}'$** geometry, spin−orbit interaction between the S_1 and T_1 excited states is absent because the direct product of irreducible representations of the SOMOs of these excited states and the orbital angular momentum operator (*l*) does not belong to the a_1 representation in the C_{2v}-symmetrical **$1S_{1a}'$** geometry; see the

---

[24] Although the MMLCT excitation decreases more the electron density of the dσ^*(Pt−Pt) orbital in the CH_3CN solution than in vacuo in both **1** and **2**, the Pt−Pt distance of the MMLCT excited state is little different in **2** between the CH_3CN solution and in vacuo, unlike **1**. This is probably because the Pt−Pt distance of the MMLCT excited state is sufficiently short in **2** even in vacuo.

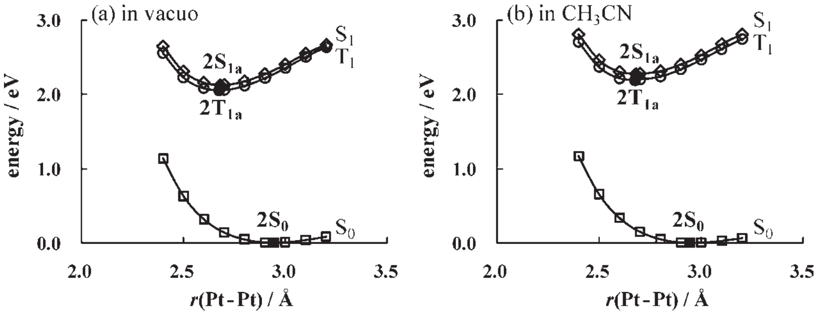

Figure 4. PECs of the S_0, T_1, and S_1 states of **2** vs the Pt−Pt distance. Geometries were optimized with the B3PW91/basis I method at each Pt−Pt distance. It is noted that the energy difference between the T_1 and S_0 curves does not correspond to the energy of phosphorescence because the T_1 curve represents the energy of the T_1-optimized geometry and the S_0 curve represents the energy of the S_0-optimized geometry. The energy of phosphorescence corresponds to the energy difference between the T_1 and S_0 states at the T_1-optimized geometry.

Supporting Information, pp S6−S13, for details. Thus, the $S_1 \rightarrow T_1$ intersystem crossing hardly occurs in the $\mathbf{1S_{1a}}'$ geometry. As a result, the population of the T_1 state is absent and the phosphorescence of **1** cannot occur in the CH_3CN solution.

Although the $S_1 \rightarrow T_1$ intersystem crossing is considered to hardly occur, the fluorescence of **1** was not experimentally observed in the CH_3CN solution.[5] This means that the $S_1 \rightarrow S_0$ nonradiative decay occurs; if not, the $S_1 \rightarrow S_0$ fluorescence spectrum must be observed. We will briefly discuss here the reason why the $S_1 \rightarrow S_0$ nonradiative decay occurs around the S_1 global minimum geometry ($\mathbf{1S_{1a}}'$) in the CH_3CN solution. The energy difference between the S_1 and S_0 states is evaluated to be small (1.33 eV) at the $\mathbf{1S_{1a}}'$ geometry with the PCM method. This energy difference becomes much smaller than 1.33 eV as the Pt−Pt distance becomes shorter than the equilibrium distance of $\mathbf{1S_{1a}}'$ (2.620 Å), as shown in Figure 3b. Because the Pt−Pt distance would become shorter by molecular vibration and/or geometry fluctuation around $\mathbf{1S_{1a}}'$, it is likely that the $S_1 \rightarrow S_0$ nonradiative transition occurs in the CH_3CN solution at RT. We discuss the reason why the shortening of the Pt−Pt distance leads to a decrease in the energy difference between the S_1 and S_0 states. The dσ*(Pt−Pt) orbital energy becomes higher as the Pt−Pt distance becomes shorter, as discussed above. Because the dσ*(Pt−Pt) orbital is doubly occupied in the S_0 state but singly occupied in the S_1 state, the S_0 state becomes more unstable in energy than the S_1 state as the Pt−Pt distance becomes shorter. Hence, the energy difference between the S_1 and S_0 states becomes small with a decrease in the Pt−Pt distance.

Here, we discuss whether the $T_1 \rightarrow S_0$ emission is allowed or forbidden; this discussion is necessary because forbidden phosphorescence is not observed at all even if the $S_1 \rightarrow T_1$ intersystem crossing occurs. The $T_1 \rightarrow S_0$ transition occurs when some of the singlet excited states mix into the T_1 state through spin−orbit interaction. As discussed above, spin−orbit interaction between the S_1 and T_1 states is absent at the $\mathbf{1T_{1a}}'$ geometry. Thus, the $S_1 \rightarrow S_0$ transition does not contribute to the oscillator strength of the $T_1 \rightarrow S_0$ emission. On the other hand, the S_2 state mixes into the T_1 state by spin−orbit interaction.[25a] The oscillator strength of the $S_2 \rightarrow S_0$ transition is moderate, which is evaluated to be 0.0170 by time-dependent (TD)-B3PW91 with the PCM method.[25b] Singlet excited states with higher energy than the S_2 state mix less into the T_1 state because the energy difference between the higher-energy singlet excited state and the T_1 state is large. In conclusion, the $T_1 \rightarrow S_0$ emission is not forbidden mainly because of mixing of the S_2 state into the T_1 state, indicating that phosphorescence is observed in CH_3CN if the population of the T_1 state is present.

Another issue to be discussed here is whether or not the $S_1 \rightarrow T_1$ intersystem crossing occurs around the S_0 geometry ($\mathbf{1S_0}$) before geometry relaxation to the global minimum. Actually, the rapid intersystem crossing is observed in some platinum(II) complexes.[26] The S_1 state is C_1-symmetrical around the $\mathbf{1S_0}$ geometry, as shown in Figure 1, in which spin−orbit interaction between the S_1 and T_1 excited states operates to induce the $S_1 \rightarrow T_1$ intersystem crossing; see the Supporting Information, pp S6−S13, for details. After this intersystem crossing, the geometry changes to the T_1 global minimum ($\mathbf{1T_{1a}}'$). The energy difference between the T_1 and S_0 states is small (1.24 eV) at the $\mathbf{1T_{1a}}'$ geometry, as discussed above about the $\mathbf{1S_{1a}}'$ geometry; see also Table 4. Thus, it is likely that the $T_1 \rightarrow S_0$ nonradiative decay occurs at the $\mathbf{1T_{1a}}'$ geometry; in other words, **1** would not be emissive in the CH_3CN solution even though the $S_1 \rightarrow T_1$ intersystem crossing occurs before the geometry change to the $\mathbf{1S_{1a}}'$ geometry in the S_1 state.

In the solid state, the phosphorescence of **1** is experimentally observed at 2.41, 2.59, and 2.73 eV at RT.[5,27] The reason why **1** is emissive in the solid state is considerably

---

[25] (a) The direct product of two SOMOs of the S_2 state, two SOMOs of the T_1 state, and the *l* operator is the a_1 representation; see the Supporting Information, pp S13−S17, for details. (b) The oscillator strength of the $S_1 \rightarrow S_0$ transition at the $\mathbf{1T_{1b}}$ geometry is 0.0313 and that of the $S_2 \rightarrow S_0$ transition is 0.0022, indicating that the $S_2 \rightarrow S_0$ transition little contributes to the oscillator strength of the $T_1 \rightarrow S_0$ transition of **1**. Although the oscillator strength is moderately larger in the $S_1 \rightarrow S_0$ transition at the $\mathbf{1T_{1b}}$ geometry than in the $S_2 \rightarrow S_0$ transition at the $\mathbf{1T_{1a}}$ geometry, it should be concluded that the oscillator strength of the $T_1 \rightarrow S_0$ transition is not zero at the $\mathbf{1T_{1a}}$ geometry.

[26] Danilov, E. O.; Pomestchenko, I. E.; Kinayyigit, S.; Gentili, P. L.; Hissler, M.; Ziessel, R.; Castellano, F. N. *J. Phys. Chem. A* **2005**, *109*, 2465.

[27] (a) In the phosphorescence spectrum of **1** observed in the solid state at RT, three split peaks were observed at 2.41, 2.59, and 2.74 eV.[5] These split peaks were understood in terms of the coupling with the breathing vibration of the aromatic ring of bpym like the other pz-bridged dinuclear platinum(II) complex **3**.[7,8] Because such vibrational coupling is not incorporated by the usual electronic structure calculation, we compare here the calculated energy of phosphorescence with the average value of these three peaks. (b) Nonradiative decay hardly occurs in the $\mathbf{1T_{1b}}$ geometry, unlike in the $\mathbf{1T_{1a}}'$ geometry, because the energy difference between the T_1 and S_0 states is considerably larger in $\mathbf{1T_{1b}}$ than in $\mathbf{1T_{1a}}'$; see Table 4.

Table 4. Energies (eV)[a] and Assignments of Phosphorescence Spectra of **1** and **2**

		energy of phosphorescence			
		calcd			
geometry	assignment	vacuo	CH_3CN	exptl[b]	
$\mathbf{1T_{1a}}'$	π^*(bpym) → dσ^*(Pt−Pt)	1.66	1.22	*c*	CH_3CN at RT
$\mathbf{1T_{1b}}$	π^*(bpym) → π(bpym) + d(Pt)	2.33	2.28	2.41, 2.59, 2.73[d]	solid state at RT
$\mathbf{2T_{1a}}$	π^*(ppy) → dσ^*(Pt−Pt)	1.75	1.87	1.89	CH_3CN at RT
				1.93	solid state at RT

[a] The energy of phosphorescence is defined as the energy difference between the T_1 and S_0 states at the T_1-optimized geometry. This energy difference was evaluated with the B3PW91/basis II//B3PW91/basis I method. [b] See refs 5 and 6 for complexes **1** and **2**, respectively. [c] Phosphorescence was not observed. [d] The peak of the phosphorescence spectrum was split. See ref 27.

interesting. The $S_0 \rightarrow S_1$ excitation occurs at the S_0 equilibrium geometry ($\mathbf{1S_0}$), like in the CH_3CN solution. However, it is likely that the geometry of the S_1 state does not change to the S_1 global minimum ($\mathbf{1S_{1a}}$) in the solid state, unlike in the CH_3CN solution. One reason is that the molecular volume considerably changes when going from the $\mathbf{1S_0}$ geometry to the $\mathbf{1S_{1a}}$; note that the molecular volume is much different between the $\mathbf{1S_{1a}}$ (606 Å^3) and $\mathbf{1S_0}$ (585 Å^3) geometries, as shown in Table 1. Such a large volume change is difficult in the solid state. Another reason is that there is a small but nonnegligible activation barrier between the $\mathbf{1S_{1a}}$ and $\mathbf{1S_{1b}}$ geometries in the S_1 PEC, as shown in Figure 3a. This activation barrier would suppress the geometry change from $\mathbf{1S_{1b}}$ to $\mathbf{1S_{1a}}$ in the solid state; hence, the geometry of the S_1 state would stay in the local minimum geometry ($\mathbf{1S_{1b}}$) in the solid state. In the C_1-symmetrical $\mathbf{1S_{1b}}$ geometry, spin−orbit interaction between the T_1 and S_1 states operates to induce the $S_1 \rightarrow T_1$ intersystem crossing because the direct product of the irreducible representations of the SOMOs in these excited states and the *l* operator belongs to the "a" representation; see the Supporting Information, pp S6−S13, for details. The geometry of the T_1 excited state would change to the $\mathbf{1T_{1b}}$ geometry even in the solid state because the molecular volume little changes in this case; the molecular volumes of the $\mathbf{1S_{1b}}$ and $\mathbf{1T_{1b}}$ geometries are almost the same and are 586 and 585 Å^3, respectively, as shown in Table 1. Thus, the population of the T_1 state would be present, and $T_1 \rightarrow S_0$ phosphorescence occurs at the $\mathbf{1T_{1b}}$ geometry. This phosphorescence is allowed because the S_1 state mixes into the T_1 state by spin−orbit coupling, and the $S_0 \rightarrow S_1$ transition is symmetry-allowed. The energy of this phosphorescence corresponds to the energy difference between the T_1 and S_0 states at the $\mathbf{1T_{1b}}$ geometry, which is evaluated to be 2.33 eV, as shown in Table 4. This value agrees well with the experimental value (2.41, 2.59, and 2.73 eV).[5,27] The phosphorescence in the solid state is assigned as the π^*(bpym) → π(bpym) + d(Pt) transition.

At the end of this section, we mention the comparison between **1** and **3** because **3** is emissive in a 2-methyltetrahydrofuran (2-MeTHF) solution, unlike **1** in a CH_3CN solution. It is likely that the geometries of the S_1 and T_1 states of **3** are C_s-symmetrical in solution.[8] In this geometry, S_1−T_1 spin−orbit interaction operates to induce the $S_1 \rightarrow T_1$ intersystem crossing. Thus, the population of the T_1 state of **3** is not zero and the $T_1 \rightarrow S_0$ emission of **3** is observed in 2-MeTHF. This is the reason why **3** is emissive in solution, although its geometry and electronic structure are similar to those of **1**.

3.5. Reasons Why the Phosphorescence Spectrum of 2 Is Observed in Both the Solid State and the CH_3CN Solution.

Photoexcitation occurs at 2.47 eV (500 nm) in the CH_3CN solution at RT.[6] The energy difference between the S_0 and S_1 states is evaluated to be 2.33 eV at the S_0 equilibrium geometry ($\mathbf{2S_0}$). This value agrees well with the experimental excitation energy. The geometry of the S_1 state is the same as the $\mathbf{2S_0}$ geometry just after photoexcitation according to the Franck−Condon principle. It is likely that the geometry changes to the S_1 global minimum ($\mathbf{2S_{1a}}$) in the CH_3CN solution. The $\mathbf{2S_{1a}}$ geometry is C_2-symmetrical and its electronic structure is the MMLCT excited state, as shown in Figure 1. Because the direct product of the irreducible representations of the SOMOs and the *l* operator belongs to the "a" representation in the C_2 symmetry, spin−orbit interaction between the S_1 and T_1 excited states operates to induce the $S_1 \rightarrow T_1$ intersystem crossing; see the Supporting Information, pp S6−S13, for details. Then, the geometry of **2** would change to the T_1 global minimum ($\mathbf{2T_{1a}}$), in which phosphorescence would occur from the T_1 excited state to the S_0 ground state. The energy of this phosphorescence is evaluated to be 1.87 eV with the PCM method, as shown in Table 4. This value agrees well with the experimental one (1.89 eV).[6] This phosphorescence is assigned as the π^*(ppy) → dσ^*(Pt−Pt) transition.[28]

It is likely that even in the solid state geometry relaxation occurs from the $\mathbf{2S_0}$ geometry to the $\mathbf{2S_{1a}}$ one, like in the CH_3CN solution, because no barrier exists between the $\mathbf{2S_0}$ and $\mathbf{2S_{1a}}$ geometries, as discussed above. Another reason is that the molecular volume changes less when going from the $\mathbf{2S_0}$ (712 Å^3) geometry to the $\mathbf{2S_{1a}}$ (698 Å^3) geometry than when going from the $\mathbf{1S_0}$ geometry to the $\mathbf{1S_{1a}}$ geometry, as shown in Table 2. In the C_2-symmetrical $\mathbf{2S_{1a}}$ geometry, the $S_1 \rightarrow T_1$ intersystem crossing occurs, followed by geometry relaxation to the $\mathbf{2T_{1a}}$ geometry on the T_1 PEC. Thus, the population of the T_1 state is present; hence, $T_1 \rightarrow S_0$ phosphorescence occurs at the $\mathbf{2T_{1a}}$ geometry in the solid state; note that this phosphorescence is allowed because the S_1 state mixes into the T_1 state through spin−orbit interaction and the S_1−S_0 transition is allowed. The energy of this phosphorescence is calculated to be 1.75 eV, as shown in Table 4. This energy agrees well with the experimental value (1.93 eV)[6] observed in the solid state.

---

(28) It is noted that the energy difference between the T_1 and S_0 states in the CH_3CN solution is considerably larger at the $\mathbf{2T_{1a}}$ geometry (1.87 eV) than at the $\mathbf{1T_{1a}}'$ geometry (1.24 eV). Thus, the $T_1 \rightarrow S_0$ nonradiative decay hardly occurs in **2**, unlike in **1**, which agrees with the experimental results that phosphorescence of **2** is observed in the CH_3CN solution.[5]

We discuss here the reason why the energy of phosphorescence of **2** is similar between in the solid state and the CH_3CN solution. The important result is that the local minimum is absent in the T_1 PEC of **2**. Another important factor is the moderate change in the molecular volume when going from the $\mathbf{2S_0}$ geometry to the $\mathbf{2T_{1a}}$ geometry. Thus, the T_1 geometry of **2** reaches almost the same global minimum geometry ($\mathbf{2T_{1a}}$) in both the solid state and the CH_3CN solution, leading to the similar energy of phosphorescence of **2** between the solid state and the CH_3CN solution. In **1**, on the other hand, the T_1 geometry still exists at the T_1 local minimum in the solid state but changes to the T_1 global minimum in a CH_3CN solution, as discussed above.

This difference between **1** and **2** arises from the different direction of the lone-pair orbitals between pz and pyt; as discussed above, the nitrogen and sulfur lone-pair orbitals of pyt expand toward rather the inside, as shown in Figure 2, while nitrogen lone-pair orbitals of pz expand toward the outside. As a result, the geometry bearing the long Pt−Pt distance can be formed in **1** but not in **2**. This is one of the important factors for the different features between **1** and **2**.

4. Conclusions

In the S_1 PEC of **1**, both global ($\mathbf{1S_{1a}}$) and local ($\mathbf{1S_{1b}}$) minimum geometries are present. The $\mathbf{1S_{1b}}$ geometry is similar to the S_0 equilibrium geometry ($\mathbf{1S_0}$), but the $\mathbf{1S_{1a}}$ geometry is considerably different. The S_1 state of **1** takes the $\mathbf{1S_{1b}}$ geometry in the solid state because the geometry changes from the $\mathbf{1S_0}$ geometry to the $\mathbf{1S_{1a}}$ one with difficulty in the solid state. Spin−orbit interaction between the T_1 and S_1 states operates in this C_1-symmetrical $\mathbf{1S_{1b}}$ geometry to induce the $S_1 \rightarrow T_1$ intersystem crossing. Then, the geometry moderately changes to the ^{3}LC/MLCT minimum geometry ($\mathbf{1T_{1b}}$), in which $\pi^*(\text{bpym}) \rightarrow \pi(\text{bpym}) + d(\text{Pt})$ phosphorescence occurs. In the CH_3CN solution, the S_1 geometry of **1** reaches the S_1 global minimum ($\mathbf{1S_{1a}}'$) concomitantly with a change of the electronic structure from the ^{1}LC/MLCT state to the ^{1}MMLCT state. Because of the C_{2v}-symmetrical $\mathbf{1S_{1a}}'$ geometry, spin−orbit interaction between the T_1 and S_1 states is absent not to induce the $S_1 \rightarrow T_1$ intersystem crossing. Also, the S_1 excited state of **1** nonradiatively decays to the S_0 ground state because of the small energy difference (1.33 eV) between the S_1 and S_0 states at the $\mathbf{1S_{1a}}'$ geometry. Thus, both phosphorescence and fluorescence of **1** are not observed in the CH_3CN solution at RT. There is a possibility that the $S_1 \rightarrow T_1$ intersystem crossing occurs before geometry relaxation to the $\mathbf{1S_{1a}}'$ geometry. Even in this case, $T_1 \rightarrow S_0$ phosphorescence is not observed in CH_3CN, too, because the $T_1 \rightarrow S_0$ nonradiative decay would easily occur because of the small energy difference between the T_1 and S_0 states at the T_1 global minimum geometry ($\mathbf{1T_{1a}}'$) in CH_3CN.

In the S_1 PEC of **2**, the local minimum is absent and the molecular volume does not change very much when going from the S_0 equilibrium geometry ($\mathbf{2S_0}$) to the S_1 global minimum geometry ($\mathbf{2S_{1a}}$). Hence, the S_1 geometry of **2** changes to the $\mathbf{2S_{1a}}$ geometry in both the solid state and the CH_3CN solution. Because the $\mathbf{2S_{1a}}$ geometry is C_2-symmetrical, spin−orbit interaction operates to induce the $S_1 \rightarrow T_1$ intersystem crossing. Thus, the population of the T_1 state is present; hence, $\pi^*(\text{ppy}) \rightarrow d\sigma^*(\text{Pt−Pt})$ phosphorescence occurs at the $\mathbf{2T_{1a}}$ geometry in both the solid state and the CH_3CN solution. The direction of lone-pair orbitals of the bridging ligand and the symmetry of the chelating ligand are responsible for these differences between **1** and **2**.

Acknowledgment. This work was financially supported by Grant-in-Aid on Priority Areas for "Molecular Theory for Real Systems" (No. 461), Grant-in-Aid on Specially Promoted Area (No. 22000009), and NAREGI Project from the Ministry of Education, Science, Sports, and Culture, and Research Fellowship of the Japan Society for the Promotion of Science for Young Scientists. Some of the theoretical calculations were performed with SGI workstations of the Institute for Molecular Science (Okazaki, Japan), and some of them were carried out with PC cluster computers in our laboratory.

Supporting Information Available: Complete ref 21, optimized bond distances in the pz and bpym rings of **1** and those in the pyt and ppy rings of **2**, orbital energies and transition energies of phosphorescences evaluated by B3PW91/basis I and B3PW91/basis II, detailed discussion about spin−orbit interaction between the S_1 and T_1 excited states, absorption and emission spectra of **1**. This material is available free of charge via the Internet at http://pubs.acs.org.